

Probing cold nuclear matter effects with the productions of isolated- γ and γ +jet in p+Pb collisions at $\sqrt{s_{NN}} = 8.16$ TeV

Guo-Yang Ma,¹ Wei Dai*,² and Ben-Wei Zhang^{†1}

¹*Key Laboratory of Quark & Lepton Physics (MOE) and Institute of Particle Physics,
Central China Normal University, Wuhan 430079, China*

²*School of Mathematics and Physics, China University of Geosciences, Wuhan 430079, China*
(Dated: November 28, 2018)

We investigate the cold nuclear matter (CNM) effects on the productions of the isolated prompt photon and γ +jet in proton-lead collisions at 8.16 TeV under the next-to-leading order (NLO) perturbative quantum chromodynamics calculations with four parametrizations for nuclear parton distribution functions (nPDFs), *i.e.* DSSZ, EPPS16, nCTEQ15, nIMParton. Our theoretical calculations provide good descriptions of pp baseline in the ATLAS collaboration and make predictions for future experimental results at p+Pb collisions. We calculate the dependence of the nuclear modification factor of isolated prompt photon on transverse momentum p_T^γ and pseudo-rapidity η^γ at very forward and backward rapidity regions, and demonstrate that the forward-to-backward yield asymmetries Y_{pPb}^{asym} as a function of p_T^γ with different nPDFs parametrizations have diverse behaviors. Furthermore, the nuclear modification factor of isolated- γ +jet $R_{pPb}^{\gamma\text{Jet}}$ as a function of γ +jet's pseudo-rapidity $\eta_{\gamma\text{Jet}} = \frac{1}{2}(\eta_\gamma + \eta_{\text{jet}})$ at different average transverse momentum $p_T^{\text{avg}} = \frac{1}{2}(p_T^\gamma + p_T^{\text{jet}})$ has been discussed, which can facilitate a tomography study of CNM effects with precise locations in a rather wide kinematic region by varying the transverse momenta and rapidities of both isolated photon and jet in p+A collisions.

PACS numbers: 12.38.Mh; 25.75.-q; 13.85.Ni

1 INTRODUCTION

In high energy nuclear physics, productions of prompt photon and photon associated jet with high transverse momentum are valuable observations of the short-distance dynamics of quarks and gluons [1]. Since prompt photon is precisely calculable by perturbative quantum chromodynamics (pQCD) at higher order corrections and carries no color charge like other gauge bosons, it has been widely regarded as an optimal probe of the initial state of the collisions[2–16], as well as an excellent tag of invasive parton (jet) to quantify the mechanisms of jet quenching in ultra-relativistic heavy ion collisions [17–22]. In the past few years, ATLAS [23–25] and CMS [15, 26–28] collaborations have made lots of measurements on isolated prompt photon and γ +jet productions in proton-proton, proton-nucleus and nucleus-nucleus collisions. The isolated photon's nuclear modification factor depending on photon transverse energy E_T^γ measured in most central PbPb collisions has large uncertainty, it also shows centrality dependence at limited E_T^γ intervals [15]. And γ +jet events have been discussed to extend the study on the tomography of quark-gluon plasma(QGP) created in heavy ion collisions. For instance, the distribution of photon plus jet transverse momentum imbalance ($x_{j\gamma} = p_T^{\text{jet}}/p_T^\gamma$) indicates that a

larger part of jet's initial energy would be damped and deposited in most central Pb+Pb collisions[20–22, 28]. In this study we may employ the productions of isolated photon and photon+jet in p+A collisions to probe the initial-state cold nuclear matter (CNM) effects.

In elementary hadron-hadron collisions, with the perturbative QCD (pQCD), the cross section of leading particle (and jet) in general could be expressed as an convolution of the parton distribution functions (PDFs), and the hard partonic cross section, and the fragmentation functions (FFs) if applicable. The parton distribution function (PDF) for a parton i from the free proton ($f_i^p(x, Q^2)$) is of nonperturbative property in the frame of the QCD collinear factorization theorem [29, 30] and its evolution in the scale Q^2 can be depicted as the DGLAP equations [31–33]. In p+A collisions, PDFs in nuclear environment should be modified due to different CNM effects, such as shadowing, anti-shadowing, EMC effect and Fermi motion *etc.* [34]. It is expected that the QCD factorization theorem may hold for nuclei as a good approximation, and we can replace the PDF in a free proton ($f_i^p(x, Q^2)$) with the nuclear PDF ($f_i^A(x, Q^2)$) to effectively include different CNM effects to study hard processes in p+A collisions.

In past three decades, our understanding on the global fits of nuclear PDFs (nPDFs) have been regularly enriched by the growing experimental results of the fixed-target deeply inelastic scattering (DIS) and low-mass Drell-Yan (DY) dilepton measurements [35–37] and the theoretical predictions from leading order (LO) up to next-to-next-to-leading order (NNLO) [38–41]. In the

*weidai@cug.edu.cn

†bwzhang@mail.ccnu.edu.cn

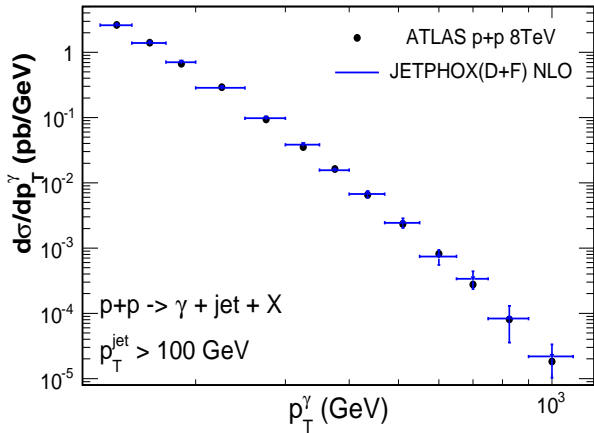


FIG. 1: The cross section of isolated photon plus jet as function of p_T^γ in $p + p$ collisions at 8 TeV and the NLO pQCD theoretical calculations(JETPHOX).

DSSZ framework [42], the global analysis for the nPDFs is presented as the ratio of parton distributions in a proton of a nucleus and in the free proton, $R_i^A(x, Q^2) = f_i^A(x, Q^2)/f_i^p(x, Q^2)$ evolving at initial scale $Q_0 = 1\text{GeV}$. The DSSZ analysis not only uses the l^\pm/μ -DIS data sets and $p+A$ DY data sets, but also firstly includes the inclusive pion production in the deuteron and gold collisions at PHENIX to constrain the nuclear gluon PDF. The EPPS16 [43] is the extension of the previous EPS09 [44] with the additional experimental data from proton-lead collisions at LHC [45–47] for the first time. It offers a less biased and favour-dependent fitting analysis for nuclear PDFs. Following the CTEQ global PDF fitting framework [39, 48, 49], nCTEQ15 [50] describes the nuclear dependence of nPDFs at NLO on different nuclei, including Pb. The nIMParton [51] is a global analysis based on two data sets of nuclear DIS data, which either only contains isospin-scalar nuclei or all nuclear data. The difference of the fitting functions obtained by these two data sets is on the shadowing (small x region) effects. In addition, the Fermi motion and off-shell effect, nucleon swelling, and parton-parton recombination are taken into account together in the nIMParton framework. In the market, some other parameterizations of nPDFs have also been proposed [52–56], and so far due to the lack of enough experimental data, limited constraints and large uncertainties appear in nuclear gluon distribution, especially at small- x and large Q^2 region, and nuclear quark distribution at large- x for all sets of nPDFs.

In this work, we study the isolated prompt photon and $\gamma + \text{jet}$ productions in proton-lead collisions at LHC energy $\sqrt{s_{\text{NN}}} = 8.16\text{TeV}$ with a NLO pQCD program JETPHOX [1, 57, 58] with updated proton's PDFs – CT14 parametrization [49]. And four sets of nuclear parton distribution functions (nPDFs) parametrizations, DSSZ, EPPS16, nCTEQ15, nIMParton, have been utilized in

obtaining the cross sections of photon and photon associated jet in $p+A$ collisions. We calculate the nuclear modification factors $R_{p\text{Pb}}$ for isolated photon production as function of transverse momentum p_T^γ and pseudo-rapidity η^γ at both forward and backward rapidity region, the forward-backward asymmetry $Y_{p\text{Pb}}^{\text{asym}}$ for isolated photon production as function of p_T^γ , and the nuclear modification factors $R_{p\text{Pb}}$ for $\gamma + \text{jet}$ production as function of $\eta_{\gamma\text{jet}}$ at limited p_T^{avg} intervals. We address the quantification of dominant Bjorken x regions detected under different specific rapidity and transverse momentum ranges.

This paper is organized as follows: in Section 2, we describe our perturbative QCD predictions of prompt photon associated jet inclusive cross section in proton-proton collisions at 8TeV. In Section 3, we discuss the nuclear modification of isolated prompt photon productions at both forward and backward region at 8.16TeV. In Section 4, the cold nuclear matter effects on photon+jet productions are studied at different transverse momentum intervals at 8.16TeV. And we give the summary in the last Section.

2 PHOTON AND PHOTON+JET PRODUCTIONS IN $P+P$

High- p_T prompt photons mainly arise from two possible mechanisms in hadronic collisions, produced directly in the hard sub-processes referred to as "direct" photons or fragmented from energetic parton. We consider that the next-to-leading order(NLO) inclusive cross section for the production of prompt photon with transverse momentum p_T^γ is given by the sum of the fragmentation and direct contributions, written as [1, 58],

$$\sigma(p_T^\gamma) = \hat{\sigma}^D(p_T^\gamma; \mu; M; M_F) + \sum_k \int_0^1 \frac{dz}{z} \hat{\sigma}^F(p_T^\gamma/z; \mu; M; M_F) D_k^\gamma(z; M_F) \quad (1)$$

Where μ is the renormalization scale, M is the initial state factorisation scale and M_F is an arbitrary final state fragmentation scale. The contribution $\hat{\sigma}^F$ denotes the partonic cross section for producing a parton convoluted with the PDF of the incoming proton, and D_k^γ is the fragmentation function of a parton k (quarks,anti-quarks and gluon) into a photon. $\hat{\sigma}^D$ includes the partonic cross section for producing a direct photon and the corresponding PDFs. Experimentally, there are also secondary photons originated from hadron decay during the collisions, therefore an isolation cut would be applied for the substantial production of photons. A photon is isolated if the amount of deposited hadronic transverse energy E_T is not more than an specific upper limit E_T^{iso} in a fixed radius $R_{\text{iso}} = \sqrt{(\eta - \eta_\gamma)^2 + (\phi - \phi_\gamma)^2}$ in pseudo-rapidity and azimuthal angle around the photon

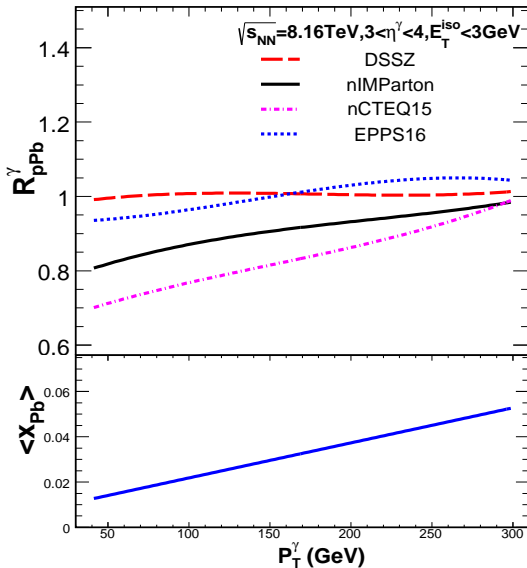


FIG. 2: (Upper) A comparison between the nuclear modification ratios R_{pPb}^{γ} for p-Pb collisions at $\sqrt{s} = 8.16$ TeV and $3 < \eta^{\gamma} < 4$ using the nCTEQ15, EPPS16, DSSZ and nIMParton nuclear modifications and the CT14 free-proton PDFs.(Bottom)The corresponding average Bjorken $\langle x_{Pb} \rangle$ as function of p_T^{γ} .

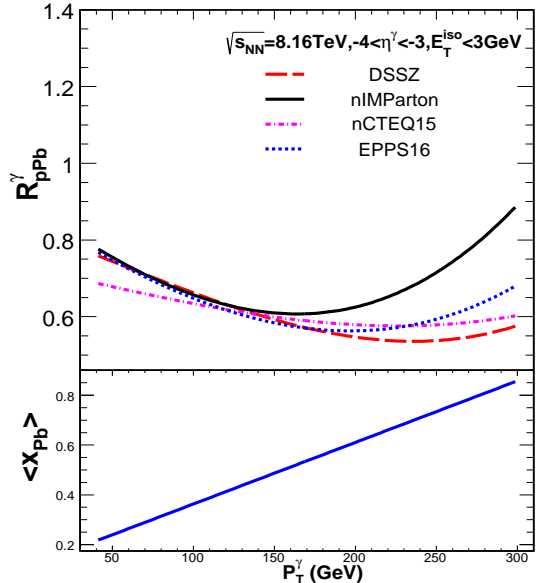


FIG. 3: The same as Fig.2, except at backward rapidity $-4 < \eta^{\gamma} < -3$.

3 ISOLATED PHOTON IN P+PB COLLISIONS AT VERY FORWARD AND BACKWARD RAPIDITY

The inclusive cross section for the isolated photon production in proton-nucleus collisions could be evaluated by using nuclear PDFs (nPDFs) as substitutes for the free-nucleon PDFs in the collinear factorization framework as stated above, which could effectively include different CNM effects.

In our calculations, we obtain the nPDFs $f_i^A(x, Q^2)$ by multiplying the CT14 parton distribution functions (PDFs)[49] with a flavor and scale dependent factor $R_i^A(x, Q^2)$ taken from four different parametrizations DSSZ [42], EPPS16 [43], nCTEQ15 [50], nIMParton [51]. These four parametrizations for nPDFs are similar that they categorize CNM effects with Bjorken x region into shadowing, anti-shadowing, EMC effect and so on, based on next-to-leading (NLO) perturbative QCD calculations, but differ in the specific formalisms and parameters for CNM effects and the input experimental data used in global fits.

The nuclear modification factors in proton+lead collisions are defined as:

$$R_{pPb} = \frac{d\sigma^{pPb}/dp_T}{\langle N_{coll} \rangle d\sigma^{pp}/dp_T} \quad (2)$$

with $\langle N_{coll} \rangle$ representing the number of binary nucleon-nucleon collisions by the glauber model [59].

Now we can make our theoretical predictions for the isolated prompt photon production in p+p and p+Pb collisions at very forward rapidity region $3 < \eta^{\gamma} < 4$

direction. This restriction on the yields of isolated photons could not only reject the secondary decay photons, but also reduce the contribution from fragmentation processes. In the following we focus on the production of isolated photon and isolated photon tagged jets in hadronic collisions.

We calculate isolated photon and jet productions in proton-proton collisions at 8TeV with a next-to-leading order pQCD program JETPHOX [1, 57, 58] with CT14 nucleon parton distribution functions [49] in accordance with the ATLAS experiment [24]. The isolated energy cut for a photon has been set as $E_T^{\text{iso}} < 6\text{GeV}$, and the isolated cone of radius in the pseudo-rapidity and azimuthal angle plane is $R_{\text{cone}} = 0.4$. Moreover photons are selected if its transverse momentum $p_T^{\gamma} > 130\text{GeV}$ and $|\eta^{\gamma}| < 2.37$, except $1.37 < |\eta^{\gamma}| < 1.56$. Jets are reconstructed by anti- k_T algorithm with cone size $R = 0.6$ with $p_T^{\text{jet}} > 100\text{GeV}$ and $|\eta^{\text{jet}}| < 4.4$. In Fig.1, we calculate the differential cross section $d\sigma/dp_T^{\gamma}$ up to $p_T^{\gamma} = 1\text{ TeV}$ in proton-proton collisions at 8 TeV, and our theoretical predication shows good agreement with the ATLAS experimental results.

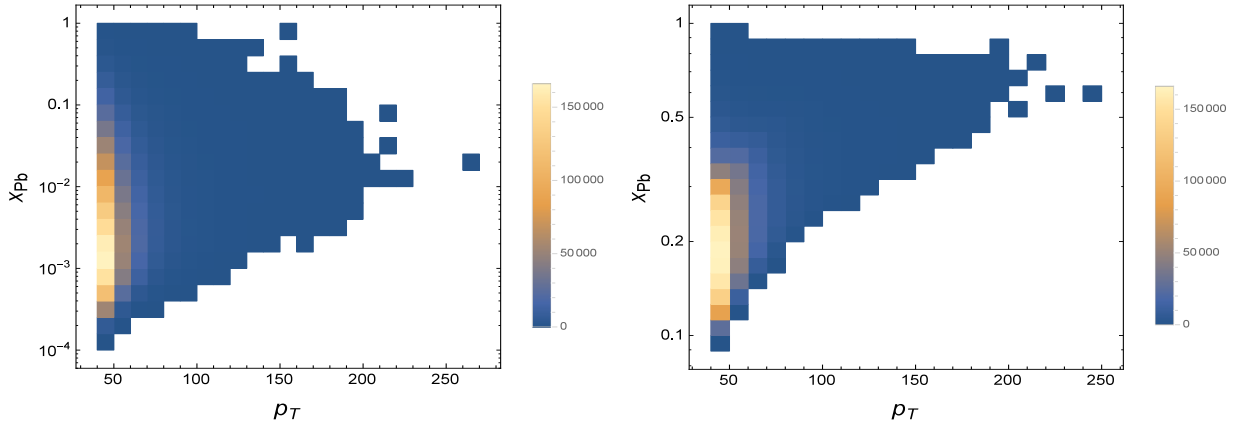


FIG. 4: (Left)NLO fluctuations at Forward rapidity $3 < \eta^\gamma < 4$; (Right)NLO fluctuations at Backward rapidity $-4 < \eta^\gamma < -3$.

at $\sqrt{s_{NN}} = 8.16\text{TeV}$ with ATLAS isolated cuts for photons [24], along with photon's transverse momentum constrained in $40\text{GeV} < p_T^\gamma < 300\text{GeV}$. We display the nuclear modification ratio $R_{p\text{Pb}}^\gamma$ as function of p_T^γ in upper panel of Fig.2. And the momentum fraction carried by initial parton from the incoming particle can be roughly estimated at LO as $x_{1,2} = 2p_T e^{\pm y}/\sqrt{s_{NN}}$, which $x_1(x_p)$ is the initial parton coming from proton on the $+z$ direction and $x_2(x_{pb})$ is the initial parton coming from lead on the $-z$ direction in $p + \text{Pb}$ collisions. The estimated average Bjorken $\langle x_{pb} \rangle$ has been defined as the events average value of Bjorken x_{pb} in JetPhox simulation. In the bottom panel of Fig.2, we show the estimation of the parton's average momentum fraction off nucleus based on NLO results with nIMParton. We have checked that $\langle x_{pb} \rangle$ varies slightly from the simulation with other nPDFs parametrizations. We can see that the average Bjorken $\langle x_{pb} \rangle$ is lower than 0.055 at very forward rapidity region, which represents the shadowing effect dominating the CNM effects. Moreover the average Bjorken $\langle x_{pb} \rangle$ has a linear positive dependence with p_T^γ expected in its LO estimation.

In the Fig.2, we see that the DSSZ's shadowing effect is unremarkable on the suppression of isolation photon production in $p + \text{Pb}$ collisions when the average Bjorken $\langle x_{pb} \rangle < 0.055$. We also notice that DSSZ's $R_{p\text{Pb}}^\gamma(p_T^\gamma)$ shows a very weak p_T^γ dependence, which means its shadowing effect is nearly independent on photon's transverse momentum in DSSZ at forward rapidity region. Meanwhile the other three parametrizations' shadowing decrease with p_T^γ increasing upon $3 < \eta^\gamma < 4$. Also we can find that the brand new nPDF parametrization nIMParton's shadowing is only weaker than nCTEQ15's in our discussion.

In Fig.3, similar phenomenon that the positively linear correlation between $\langle x_{pb} \rangle$ and p_T^γ has been shown at backward rapidity $-4 < \eta^\gamma < -3$. Whereas the estimated average Bjorken $\langle x_{pb} \rangle$ ranges from 0.25 to 0.8, which mostly correspond to EMC effect. We could go a

little further to distinguish four different parametrizations' EMC maximum from each nuclear modification factor's extreme point, such as the nIMParton's EMC minimum appears in $p_T^\gamma = 150\text{GeV}$ and the corresponding average Bjorken locates around $\langle x_{pb} \rangle = 0.5$, which is the lowest in our results. Though there is one-to-one correspondence between x_{pb} and p_T^γ at fixed rapidity in LO, this correspondence will fail at next-to-leading order accuracy, and we investigate the NLO correlations between x_{pb} and p_T^γ at both forward and backward rapidities, shown in Fig. 4. We observe the broadening of Bjorken x_{pb} at specific p_T^γ interval due to higher corrections, and the spreading of x_{pb} at small p_T^γ is rather wider. Also we can see a very dense statistics cluster around the low p_T^γ in our Monte-Carlo simulation, because the possibility distribution of the hard sub-processes for the photon production following double-logarithmic declining with photon's transverse momentum.

Note the nuclear modification factor is sensitive to the nucleon PDF(nPDF) and $p + p$ baseline [5–9, 60, 61], we may calculate the ratio of the photon production at forward and backward rapidity, which could get rid of the large uncertainty in free nucleon PDFs, which could be used to probe the CNM effects with less arbitrariness[12–14]. We define the forward-backward yield asymmetry as:

$$Y_{p\text{Pb}}^{\text{asym}} = \frac{d\sigma/dp_T(p + \text{Pb} \rightarrow \gamma + \text{X})|_{\eta \in [\eta_1, \eta_2]}}{d\sigma/dp_T(p + \text{Pb} \rightarrow \gamma + \text{X})|_{\eta \in [-\eta_2, -\eta_1]}} \quad (3)$$

Our predictions of the forward-to-backward yield asymmetries $Y_{p\text{Pb}}^{\text{asym}}$ for the isolated prompt photon production in $p + \text{Pb}$ collisions at $\sqrt{s} = 8.16\text{TeV}$ and $3 < |\eta^\gamma| < 4$ are shown in Fig.5. As a result of the symmetry of the colliding system, there is nearly no forward-to-backward yield asymmetry observed in proton-proton collisions. $Y_{p\text{Pb}}^{\text{asym}}$ is larger than one in $p + \text{Pb}$ collisions, which means the photon production suffering more suppression in the backward rapidity region. And the EMC effect reduces the photon production more effectively

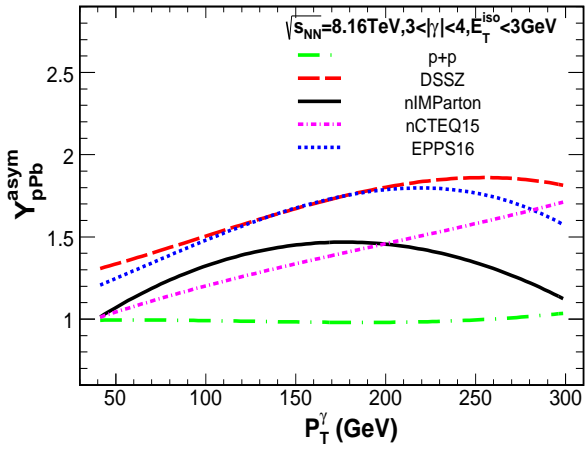


FIG. 5: A comparison between the forward-to-backward asymmetry $Y_{\text{pPb}}^{\text{asym}}$ for p-Pb collisions at $\sqrt{s_{\text{NN}}} = 8.16$ TeV and $3 < \eta^\gamma < 4$ using the nCTEQ15, EPPS16, DSSZ and nIMParton nuclear modifications and the CT14 free-proton PDFs.

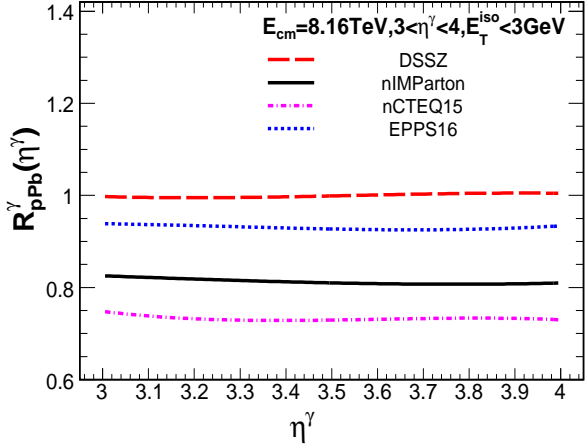


FIG. 6: The same as Fig.2, but as a function of photon's rapidity η^γ .

than the shadowing effect does on the whole. Besides, we notice that the value of $Y_{\text{pPb}}^{\text{asym}}$ starts going down to one with all parametrizations due to the decreasing of EMC effect at relatively high p_T^γ . This manifestation seems less obvious in nCTEQ15 as its EMC maximum is close to p_T^γ 's highest boundary and our approximate curve fitting.

In order to further explore the impact of input nuclear modifications on the cross section of isolated prompt photon productions in proton-nucleus collision. We further discuss the isolated photon's nuclear modification factor $R_{\text{pPb}}^\gamma(\eta^\gamma)$ as a function of photon's rapidity η^γ at both forward and backward rapidities. The Fig.6 tells us that a growing suppression on the photon productions from DSSZ, EPPS16, nIMParton and nCTEQ15

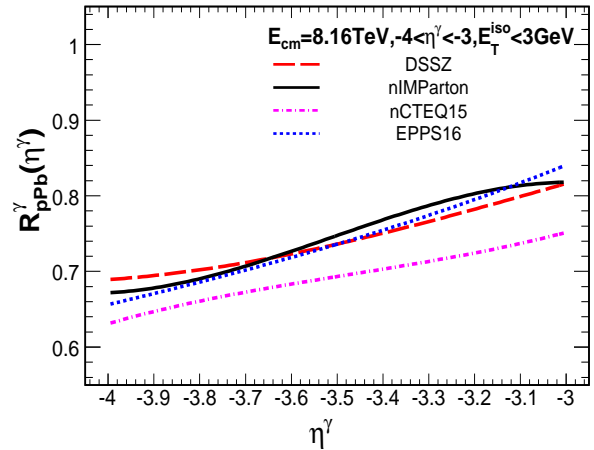


FIG. 7: The same as Fig.3, but as a function of photon's rapidity η^γ .

at forward pseudo-rapidity, which quantitatively appears in accordance with the $R_{\text{pPb}}^\gamma(p_T^\gamma)$ at $p_T^\gamma = 50\text{GeV}$ due to the highest statistics at lowest p_T^γ region in Monte-Carlo simulations exhibited above in Fig.2. On the other hand, $R_{\text{pPb}}^\gamma(\eta^\gamma)$ shows very weak η^γ dependence, because the changes on Bjorken x_{Pb} is only several thousandths at $3 < \eta^\gamma < 4$. At backward rapidity region, the nuclear modification factors using four different nPDFs all show the positive linear relation with η^γ because of a few tenths of decrease of Bjorken x_{Pb} when η^γ increase to -3 from -4 , shown in Fig.7 and Fig.3 respectively. And the nCTEQ15 parametrization gives a stronger suppression than the others', which could be confirmed in the prediction of $R_{\text{pPb}}^\gamma(p_T^\gamma)$ at low p_T^γ region in Fig.3.

4 ISOLATED PHOTON+JET IN P+PB

As compared to isolated photon productions, the isolated photon associated jet production in p+A reactions has more leverage power to access CNM effects in a wider kinematic regions due to its exclusive property. To understand the nuclear modifications for isolated prompt photon associated jet productions, one usually estimates the momentum fractions of the initial-state partons at leading order(LO) to evaluate the CNM effects' contribution by the final-state kinematics, namely $x_{1,2}$ defined above. In the following, we are enlightened by the work on dijets productions in the CMS collaboration [62]. and provide the $\gamma+\text{jet}$ pseudo-rapidity $\eta_{\gamma\text{jet}} = \frac{1}{2}(\eta_\gamma + \eta_{\text{jet}})$ distributions of a photon tagged jet at specific range of their average transverse momentum $p_T^{\text{avg}} = \frac{1}{2}(p_T^\gamma + p_T^{\text{jet}})$. As $\eta_{\gamma\text{jet}}$ would be equal to $\frac{1}{2}\ln(x_p/x_{\text{Pb}})$ in the center-of-mass frame when two partons collide with each other at LO. The NLO simulation would give rise to complicated correlations between x_{Pb} (x_p) and $\eta_{\gamma\text{jet}}$ describing the nu-

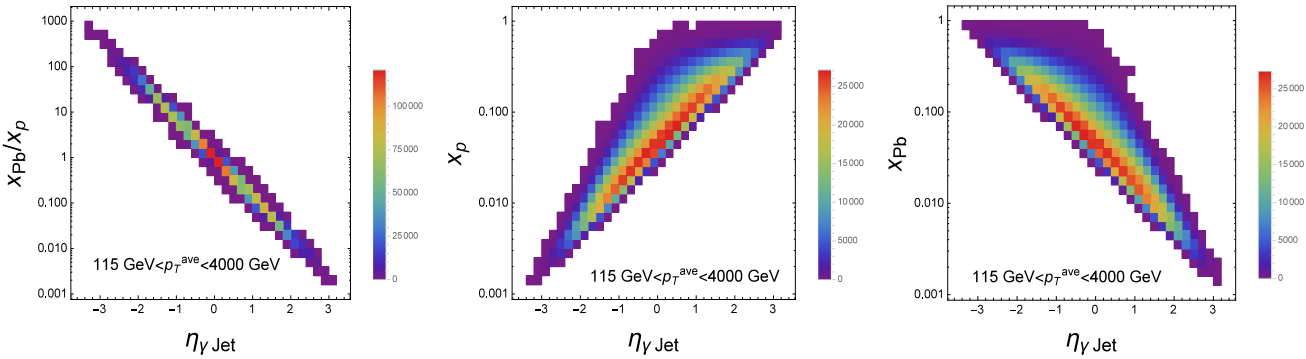


FIG. 8: Correlation between x_{Pb}/x_p (Left), x_p (Middle), x_{Pb} (Right) and $\gamma+\text{jet}$ pseudorapidity $\eta_{\gamma\text{jet}}$.

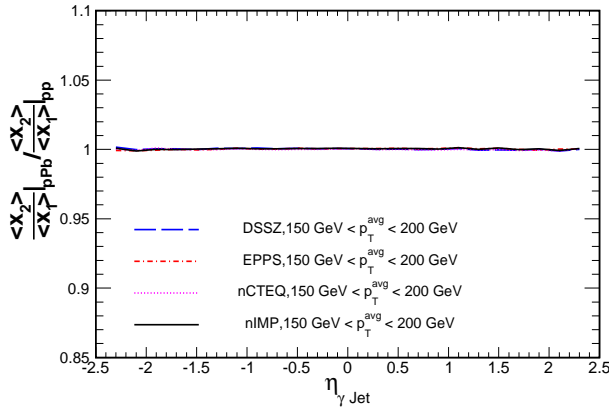


FIG. 9: The ratio of $\langle x_2 \rangle$ in p+Pb and p+p collisions as a function of $\eta_{\gamma\text{jet}}$, considering different CNM effects descriptions.

clear matter's influence, shown in Fig. 8 (with nIMParton nPDFs). We also compute the correlations between x_{Pb}/x_p and $\eta_{\gamma\text{jet}}$ at $115\text{GeV} < p_{\text{T}}^{\text{avg}} < 4000\text{GeV}$ interval in Fig. 8. It is shown though at NLO accuracy, both distributions of x_{Pb} and x_p over $\eta_{\gamma\text{jet}}$ are rather wider, when the ratio x_{Pb}/x_p at NLO is rather narrow and centered at values at LO with very high statistics.

In Fig.9, we can notice that there are tiny shifts on $\frac{\langle x_2 \rangle}{\langle x_1 \rangle}$ as a function of $\eta_{\gamma\text{jet}}$ caused by nuclear matter. Based on the relation between $\eta_{\gamma\text{jet}}$ and $\langle x_{\text{Pb}} \rangle$ we could reach an assessment about different CNM effects predominate region at $\eta_{\gamma\text{jet}}$, which the $\gamma+\text{jet}$ production is sensitive to shadowing ($\eta_{\gamma\text{jet}} > 1.6$), anti-shadowing ($-0.2 < \eta_{\gamma\text{jet}} < 1.6$), and EMC effects ($\eta_{\gamma\text{jet}} < -0.2$) at $150 < p_{\text{T}}^{\text{avg}} < 200$ interval, shown as the black line in Fig.10. The average Bjorken $\langle x_{\text{Pb}} \rangle$ shows a nearly negative linear relation with $\eta_{\gamma\text{jet}}$, and becomes globally higher when the $p_{\text{T}}^{\text{avg}}$ interval increasing.

Furthermore, we discuss the nuclear modification factor for $\gamma+\text{jet}$ production as a function of $\eta_{\gamma\text{jet}}$ at $115\text{GeV} < p_{\text{T}}^{\text{avg}} < 4000\text{GeV}$ and $200\text{GeV} < p_{\text{T}}^{\text{avg}} <$

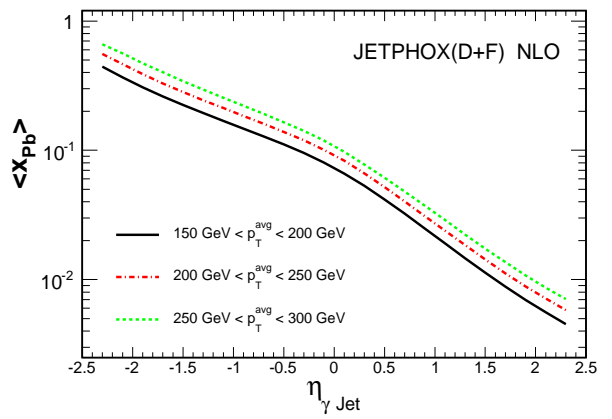


FIG. 10: Mean Bjorken x of the parton from the lead ion x_{Pb} obtained from JetPhox with nIMParton as a function of $\eta_{\gamma\text{jet}}$ in different $\gamma+\text{jet}$ events' $p_{\text{T}}^{\text{avg}}$ intervals.

250GeV . We have roughly estimated that the nuclear modification factor is sensitive to shadowing when $\eta_{\gamma\text{jet}} > 1.6$ and is sensitive to EMC effect when $\eta_{\gamma\text{jet}} < -0.2$. In the total average transverse momentum interval ($115\text{GeV} < p_{\text{T}}^{\text{avg}} < 4000\text{GeV}$), we could find that nIMParton offers the strongest shadowing effect, and EPPS16 has the most predominant anti-shadowing effect and EMC effect, along with DSSZ's is in between these two. At the meantime, nCTEQ15 provides a almost constant suppression when $\eta_{\gamma\text{jet}}$ varies. When the average transverse momentum interval limited to $200\text{GeV} < p_{\text{T}}^{\text{avg}} < 250\text{GeV}$, nCTEQ15's shadowing starts to restore, as well as it remains flattened at small $\eta_{\gamma\text{jet}}$ and large average Bjorken $\langle x_{\text{Pb}} \rangle$. nIMParton's and EPPS16's shadowing becomes more damped. And EPPS16 has more clear anti-shadowing peak as well as nIMParton and DSSZ begin to reveal anti-shadowing peak. DSSZ provides the strongest EMC suppression at this situation. It is emphasized by leveraging the rapidity and transverse momentum of both photon and jets with measured $p_{\text{T}}^{\text{avg}}$ and $\eta_{\gamma\text{jet}}$, we can get access to CNM effects in a wide

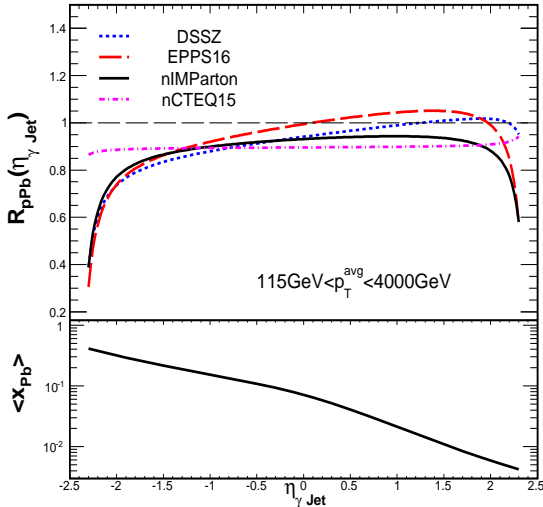


FIG. 11: (Upper) The nuclear modification factor for γ +jet production as a function of $\eta_{\gamma\text{jet}}$ at $115\text{GeV} < p_T^{\text{avg}} < 4000\text{GeV}$. The NLO pQCD calculation is based on JetPhox with nCTEQ15, EPPS16, DSSZ and nIMParton as the nPDFs. (Bottom) The corresponding average Bjorken $\langle x_{\text{Pb}} \rangle$ as function of $\eta_{\gamma\text{jet}}$ based on nIMParton.

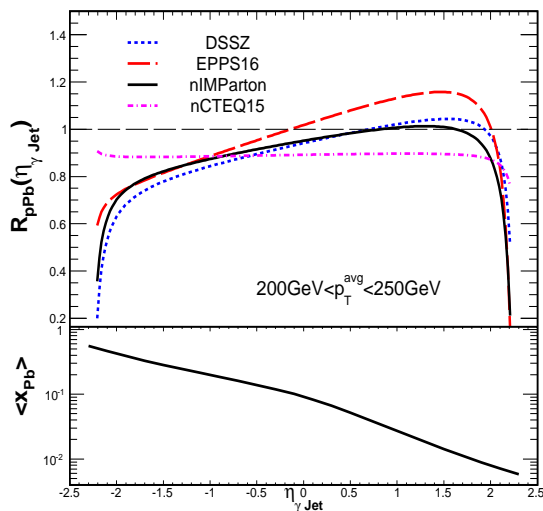


FIG. 12: The same as Fig.11, except for at $200\text{GeV} < p_T^{\text{avg}} < 250\text{GeV}$

regime and also allocate different kinematics precisely, where differences between varieties of nPDFs sets may be investigated more effectively.

5 SUMMARY

We calculate the productions of isolated prompt photon and γ + jet in p+A with CNM effects from four

sets of nuclear parton distribution functions (nPDFs) parametrizations, *i.e.* DSSZ, EPPS16, nCTEQ15, nIMParton, by utilizing the NLO pQCD approach at LHC 8.16 TeV. We present the nuclear modification ratio of isolated prompt photon $R_{\text{pA}}^{\gamma}(p_T^{\gamma})$ and $R_{\text{pA}}^{\gamma\gamma}(\eta^{\gamma\gamma})$, and find shadowing effect and EMC effects dominating at very forward and backward rapidity region respectively. And the rapidity dependence of prompt photon's nuclear modification ratio shows weak rapidity dependence at forward region and varies linearly at backward rapidity region. The production of the isolated photon associated with jet gives us the leveraged power to study the tomography of cold nuclear matter. And the CNM effects of γ +jet productions could be intuitively presented at constraint rapidity $\eta_{\gamma\text{jet}}$ and average transverse momentum p_T^{avg} region in our discussion. In terms of sensitivity, comparisons of four different nPDFs parametrization's cold nuclear matter contribution have been exhibited, and nCTEQ15 shows peculiar results than the others, which could extend our understanding on the constraints of different nPDFs descriptions. It is noted in our work the nPDF parametric form (nIMParton) proposed by Institute of Modern Physics in China has been applied for the first time to investigate hard processes in ultra-relativistic heavy-ion collisions, with a comparison again other three mainstream nPDF groups' predictions.

Acknowledgments: This research is supported by the NSFC of China with Project Nos. 11435004, 11805167 and partly supported by China University of Geosciences (Wuhan) (No. 162301182691).

- [1] S. Catani, M. Fontannaz, J. P. Guillet and E. Pilon, JHEP **0205**, 028 (2002) [hep-ph/0204023].
- [2] I. Vitev and B. W. Zhang, Phys. Lett. B **669**, 337 (2008) [arXiv:0804.3805 [hep-ph]].
- [3] R. B. Neufeld, I. Vitev and B. W. Zhang, Phys. Lett. B **704**, 590 (2011) [arXiv:1010.3708 [hep-ph]].
- [4] F. Arleo, K. J. Eskola, H. Paukkunen and C. A. Salgado, JHEP **1104**, 055 (2011) [arXiv:1103.1471 [hep-ph]].
- [5] J. L. Albacete *et al.*, Int. J. Mod. Phys. E **22**, 1330007 (2013) doi:10.1142/S0218301313300075 [arXiv:1301.3395 [hep-ph]].
- [6] J. L. Albacete *et al.*, Int. J. Mod. Phys. E **25**, no. 9, 1630005 (2016) doi:10.1142/S0218301316300058 [arXiv:1605.09479 [hep-ph]].
- [7] J. L. Albacete *et al.*, Nucl. Phys. A **972**, 18 (2018) [arXiv:1707.09973 [hep-ph]].
- [8] P. Ru, B. W. Zhang, L. Cheng, E. Wang and W. N. Zhang, J. Phys. G **42**, no. 8, 085104 (2015) [arXiv:1412.2930 [nucl-th]].
- [9] P. Ru, B. W. Zhang, E. Wang and W. N. Zhang, Eur. Phys. J. C **75**, no. 9, 426 (2015) [arXiv:1505.08106 [nucl-th]].
- [10] P. Ru and B. W. Zhang, Nucl. Part. Phys. Proc. **289-290**, 197 (2017) [arXiv:1612.02899 [nucl-th]].
- [11] P. Ru, S. A. Kulagin, R. Petti and B. W. Zhang, Phys. Rev. D **94**, no. 11, 113013 (2016) [arXiv:1608.06835 [nucl-th]].
- [12] I. Helenius, K. J. Eskola and H. Paukkunen, JHEP **1409**,

138 (2014) [arXiv:1406.1689 [hep-ph]].

[13] M. Goharipour and H. Mehraban, Phys. Rev. D **95**, no. 5, 054002 (2017) [arXiv:1702.05738 [hep-ph]].

[14] M. Goharipour and S. Rostami, arXiv:1808.05639 [hep-ph].

[15] S. Chatrchyan *et al.* [CMS Collaboration], Phys. Lett. B **710**, 256 (2012) [arXiv:1201.3093 [nucl-ex]].

[16] P. Janus *et al.* [ATLAS Collaboration], KnE Energ. Phys. **3**, 345 (2018).

[17] X. N. Wang and Z. Huang, Phys. Rev. C **55**, 3047 (1997) [hep-ph/9701227].

[18] X. N. Wang, Z. Huang and I. Sarcevic, Phys. Rev. Lett. **77**, 231 (1996) [hep-ph/9605213].

[19] W. Dai, S. Y. Chen, B. W. Zhang and E. K. Wang, Commun. Theor. Phys. **59**, 349 (2013).

[20] W. Dai, I. Vitev and B. W. Zhang, Phys. Rev. Lett. **110**, no. 14, 142001 (2013) [arXiv:1207.5177 [hep-ph]].

[21] X. N. Wang and Y. Zhu, Phys. Rev. Lett. **111**, no. 6, 062301 (2013) [arXiv:1302.5874 [hep-ph]].

[22] T. Luo, S. Cao, Y. He and X. N. Wang, Phys. Lett. B **782**, 707 (2018) [arXiv:1803.06785 [hep-ph]].

[23] M. Aaboud *et al.* [ATLAS Collaboration], Phys. Lett. B **770**, 473 (2017) [arXiv:1701.06882 [hep-ex]].

[24] M. Aaboud *et al.* [ATLAS Collaboration], Nucl. Phys. B **918**, 257 (2017) [arXiv:1611.06586 [hep-ex]].

[25] The ATLAS collaboration [ATLAS Collaboration], ATLAS-CONF-2017-072.

[26] A. M. Sirunyan *et al.* [CMS Collaboration], arXiv:1807.00782 [hep-ex].

[27] A. M. Sirunyan *et al.* [CMS Collaboration], arXiv:1801.04895 [hep-ex].

[28] A. M. Sirunyan *et al.* [CMS Collaboration], Phys. Lett. B **785**, 14 (2018) [arXiv:1711.09738 [nucl-ex]].

[29] J. C. Collins, D. E. Soper and G. F. Sterman, Adv. Ser. Direct. High Energy Phys. **5**, 1 (1989) [hep-ph/0409313].

[30] R. Brock *et al.* [CTEQ Collaboration], “Handbook of perturbative QCD; Version 1.1: September 1994.”

[31] Y. L. Dokshitzer, Sov. Phys. JETP **46**, 641 (1977) [Zh. Eksp. Teor. Fiz. **73**, 1216 (1977)].

[32] V. N. Gribov and L. N. Lipatov, Sov. J. Nucl. Phys. **15**, 438 (1972) [Yad. Fiz. **15**, 781 (1972)].

[33] G. Altarelli and G. Parisi, Nucl. Phys. B **126**, 298 (1977).

[34] D. de Florian and R. Sassot, Phys. Rev. D **69**, 074028 (2004) [hep-ph/0311227].

[35] K. J. Eskola, V. J. Kolhinen and C. A. Salgado, Eur. Phys. J. C **9**, 61 (1999) [hep-ph/9807297].

[36] K. J. Eskola, Nucl. Phys. A **910-911**, 163 (2013) [arXiv:1209.1546 [hep-ph]].

[37] H. Paukkunen, Nucl. Phys. A **926**, 24 (2014) [arXiv:1401.2345 [hep-ph]].

[38] J. Pumplin, D. R. Stump, J. Huston, H. L. Lai, P. M. Nadolsky and W. K. Tung, JHEP **0207**, 012 (2002) [hep-ph/0201195].

[39] J. Gao *et al.*, Phys. Rev. D **89**, no. 3, 033009 (2014) [arXiv:1302.6246 [hep-ph]].

[40] R. D. Ball *et al.* [NNPDF Collaboration], JHEP **1504**, 040 (2015) [arXiv:1410.8849 [hep-ph]].

[41] L. A. Harland-Lang, A. D. Martin, P. Motylinski and R. S. Thorne, Eur. Phys. J. C **75**, no. 5, 204 (2015) [arXiv:1412.3989 [hep-ph]].

[42] D. de Florian, R. Sassot, P. Zurita and M. Stratmann, Phys. Rev. D **85**, 074028 (2012) [arXiv:1112.6324 [hep-ph]].

[43] K. J. Eskola, P. Paakkinnen, H. Paukkunen and C. A. Salgado, Eur. Phys. J. C **77**, no. 3, 163 (2017) [arXiv:1612.05741 [hep-ph]].

[44] K. J. Eskola, H. Paukkunen and C. A. Salgado, JHEP **0904**, 065 (2009) [arXiv:0902.4154 [hep-ph]].

[45] S. Chatrchyan *et al.* [CMS Collaboration], Eur. Phys. J. C **74**, no. 7, 2951 (2014) [arXiv:1401.4433 [nucl-ex]].

[46] V. Khachatryan *et al.* [CMS Collaboration], Phys. Lett. B **750**, 565 (2015) [arXiv:1503.05825 [nucl-ex]].

[47] G. Aad *et al.* [ATLAS Collaboration], Phys. Rev. C **92**, no. 4, 044915 (2015) [arXiv:1507.06232 [hep-ex]].

[48] K. Kovarik, T. Jezo, A. Kusina, F. I. Olness, I. Schienbein, T. Stavreva and J. Y. Yu, PoS DIS **2013**, 274 (2013) [arXiv:1307.3454 [hep-ph]].

[49] S. Dulat *et al.*, EPJ Web Conf. **120**, 07003 (2016).

[50] A. Kusina *et al.*, PoS DIS **2015**, 041 (2015) [arXiv:1509.01801 [hep-ph]].

[51] R. Wang, X. Chen and Q. Fu, Nucl. Phys. B **920**, 1 (2017) [arXiv:1611.03670 [hep-ph]].

[52] S. Atashbar Tehrani, Phys. Rev. C **86**, 064301 (2012).

[53] M. Hirai, S. Kumano and T.-H. Nagai, Phys. Rev. C **76**, 065207 (2007) [arXiv:0709.3038 [hep-ph]].

[54] S. Atashbar Tehrani, arXiv:1712.02153 [hep-ph].

[55] S. A. Kulagin and R. Petti, Nucl. Phys. A **765**, 126 (2006) [hep-ph/0412425].

[56] S. A. Kulagin and R. Petti, Phys. Rev. C **90**, no. 4, 045204 (2014) [arXiv:1405.2529 [hep-ph]].

[57] P. Aurenche, M. Fontannaz, J. P. Guillet, E. Pilon and M. Werlen, Phys. Rev. D **73**, 094007 (2006) [hep-ph/0602133].

[58] Z. Belghobsi, M. Fontannaz, J.-P. Guillet, G. Heinrich, E. Pilon and M. Werlen, Phys. Rev. D **79**, 114024 (2009) [arXiv:0903.4834 [hep-ph]].

[59] D. G. d’Enterria, nucl-ex/0302016.

[60] CMS Collaboration [CMS Collaboration], CMS-PAS-HIN-12-017.

[61] Y. He, B. W. Zhang and E. Wang, Eur. Phys. J. C **72**, 1904 (2012) [arXiv:1110.6601 [hep-ph]].

[62] A. M. Sirunyan *et al.* [CMS Collaboration], arXiv:1805.04736 [hep-ex].